Carbohydrate Polymers 76 (2009) 585–592

Contents lists available at ScienceDirect

Carbohydrate Polymers

journal homepage: www.elsevier.com/locate/carbpol

Synthesis and characterization of NaMt biocomposites with corn cob xylan in aqueous media

Cüneyt H. Ünlü [a], Ebru Günister [b], Oya Atıcı [a,*]

[a] Istanbul Technical University, Faculty of Science and Letters, Department of Chemistry, Maslak TR 34469, Istanbul, Turkey
[b] Istanbul Technical University, Faculty of Science and Letters, Department of Physics, Maslak TR 34469, Istanbul, Turkey

ARTICLE INFO

Article history:
Received 5 September 2008
Received in revised form 13 November 2008
Accepted 18 November 2008
Available online 3 December 2008

Keywords:
Xylan
Montmorillonite
Biocomposite
Spectroscopy
Rheology
Thermal analysis
Morphology

ABSTRACT

In this study synthesis and characterization of biopolymer/clay biocomposites was aimed using naturally occurring polysaccharide (xylan) as biopolymer and montmorillonite type clay (NaMt). Xylan was extracted from corn cobs via alkaline oxidative treatment. Maximum solubility of xylan was determined as 1% (w/v) in water at room temperature. Thus synthesis was realized following two routes; first NaMt concentration was kept constant at 2.0×10^{-2} g/ml and xylan concentration was changed. Latter xylan concentration was kept constant at 1.0×10^{-2} g/ml and NaMt concentration was changed. Natural xylan, NaMt and biocomposites were examined in terms of their spectral, electrokinetic, rheologic, morphologic and thermal properties. Results showed that lower amounts of xylan interacted with NaMt on the surface, however, when the xylan amount was increased also intercalation of NaMt has occurred. Biocomposites showed better thermal and rheologic behaviors with respect to the starting materials.

© 2008 Elsevier Ltd. All rights reserved.

1. Introduction

Corn cob, which is a very rich resource for xylan, is a waste material of oil and starch production. Xylan is one of the major components of corn cob with a ratio 25–35% and it is one of the most studied polysaccharides in recent years (Ebringerová, Hromádková, & Heinze, 2005; Kacurakova, Capek, Sasinkova, Wellner, & Ebringerova, 2000; Kacuráková, Belton, Wilson, Hirsch, & Ebringerová, 1998; Sun & Tomkinson, 2002). Xylans of the terrestrial plants are heteropolymers possessing a β-(1-4)-D-xylopyranose backbone, which is branched by short carbohydrate chains which has a helical structure. Corn cob xylan, also referred as corn fiber gum, is a quite sticky polymer. Therefore it could serve as adhesive, thickener (Doner & Hicks, 1997), additive to plastics (due to increasing their stretch, breaking resistance, and makes them more susceptible to biodegradation) (Gáspár, Juhász, Szengyel, & Réczey, 2005), food additive (due to its emulsifying activity and ability to stabilize protein foam during heating) (Hromadkova, Kovacikova, & Ebringerova, 1999). The diversity and complexity of xylans suggest that many useful by-products can be potentially produced and, therefore, these polysaccharides are considered as possible biopolymer raw materials for various exploitations (Ebringerová et al., 2005).

Another popular subject is polymer/clay nanocomposites nowadays. First research about this subject was made by Toyota Research Group in 1990s and then many researches have been made about this subject in both academic and industrial areas in recent years (Ray & Bousmina, 2005; Ray & Okamoto, 2003). The use of clay in making nanocomposite has recently been increased because of the cheap and easy provide of it. Smectite-group clay minerals have large adsorption capacities for polymer molecules due to their unique crystal structure. Montmorillonite is a member of the smectite-group minerals and has a layered structure and it is the most widely used layered silicate in polymer nanocomposite. The polymers in the montmorillonite dispersions interact with the clay particles, according to their ionic or non-ionic character. The ionic polymers induce electrostatic interactions, but the non-ionic polymers are adsorbed on the surface of clay minerals by the steric interactions. Polymer concentration, its molecular weight and hydrolyzing groups of polymer, size and shape of clay particle, its surface charge, clay concentration in suspension, pH, and temperature may all affect the clay/polymer interactions. The adsorption of polymers onto the surfaces of clay particles influences the rheologic and electrokinetic properties of the dispersion. In a polymer/clay nanocomposite, polymer chains are wanted to be located in the interlayer galleries of clay (Fahmy & Mobarak, 2008; Günister, Pestreli, Ünlü, Atıcı, & Güngör, 2007) resulting in an increase in basal spacing of montmorillonite (intercalation). The polymer even can cause separation of clay layers giving an exfoliated structure.

In this work, xylan from corn cob is studied for an alternative application, polymer/clay biocomposite synthesis. In our study interactions between clay and xylan are observed. A biocomposite

* Corresponding author. Tel.: +90 212 2853228; fax: +90 212 2856386.
E-mail address: atici@itu.edu.tr (O. Atıcı).

0144-8617/$ - see front matter © 2008 Elsevier Ltd. All rights reserved.
doi:10.1016/j.carbpol.2008.11.029

dispersion between xylan and clay forms with these interactions. Characterizations of the biocomposite dispersions have been made in terms of rheologic, thermal, morphologic and spectral properties.

2. Experimental

2.1. Materials

Corn cobs collected locally from Adapazarı, Turkey and clay mineral obtained from Ünye, Turkey. Chemical analyses of clay mineral were performed using a Perkin-Elmer 3030 model atomic absorption spectrophotometer. The clay sample had the chemical composition (wt.%): SiO_2 70.30; Al_2O_3 15.00; Fe_2O_3 1.10; CaO 1.60; MgO 2.30; Na_2O 1.45; K_2O 1.20; TiO_2 0.30, ignition loss 6.45.

FTIR spectra were recorded on Thermo Nicolet 380 in 4000–400 cm^{-1} region, using KBr pellets with 1% (w/w) sample concentration.

X-ray diffraction measurements were performed on Philips PW1140 model X-ray diffractometer at room temperature using Ni-filtered Cu Kα radiation.

Scanning electron microscopy (SEM) measurements were performed on Jeol JSM 6335F field emission scanning electron microscope. Samples were coated with gold–palladium alloy with a thickness of 4 nm.

The flow behavior of dispersions was determined with Brookfield DV-III low-shear rheometer. The rheologic behavior of the clay suspensions was obtained by shear stress–shear rate measurements within 0–330 s^{-1} shear rates with SSA-18 spindle. Rheologic measurements were carried out in duplicate.

The zeta potential measurements were carried out using a Malvern Instruments, Zetasizer 2000. The optic unit contains a 5 mW He–Ne (638 nm) laser. Before the measurements, all the dispersions were centrifuged at 6000 rpm for 30 min. Supernatants were then used for zeta potential measurements.

The thermal analyses were performed under N_2 atmosphere on TA Instruments Q50 from 25 to 800 °C with a heating rate of 20 °C/min (TGA) and TA Instruments Q10 from −50 to 450 °C with a heating rate of 10 °C/min (DSC).

2.2. Extraction and characterization of xylan

Ground corn cobs were suspended in distilled water. Then pH of the dispersion was adjusted to 12 with 10% (w/v) aqueous NaOH, and peroxide concentration adjusted to 0.9% with 35% (w/v) aqueous H_2O_2. Xylan was extracted from corn cob under these conditions for 3 h at 60 °C. After extraction period was over residual cellulose was filtrated, and pH of the supernatant was adjusted to 5 with 4N HCl. Then xylan was precipitated from this solution pouring it to 2.5 volumes of isopropanol. Isolated xylan was washed with isopropanol, and dried first in air, then in vacuum. Neutral sugar composition of xylan was determined with HPLC (Shimadzu SCL-10 AVP instrument, Aminex HPX-87H column, 65 °C column temperature, 0.6 ml/min flow rate, 5 mM H_2SO_4 eluent). Uronic acid content was determined with *m*-hydroxyphenol method using Jenway 6107 model UV–visible spectrophotometer (Blumenkrantz & Asboe-Hansen, 1973). Neutral sugar content of isolated xylans was determined as: (w/w) 66.4% xylose, 19.5% arabinose, 5.4% galactose by using HPLC and glucuronic acid content as 4.8% (w/w) by using colorimetric method. Molecular weights and degree of polymerization of isolated xylans were determined via intrinsic viscosity measurement using Ubbelohde Typ I capillary viscosimeter at 25 °C, 0.5N NaOH as solvent. Mark–Houwink equation was given as $[\eta] = 2.67 \times 10^{-4} M_v^{0.73}$ dl/g and $[\eta] = 9.2 \times 10^{-3} DP_v^{0.84}$ dl/g (Eremeeva & Bykova, 1993). Molecular weight and degree of polymerization was determined as 20 kDa.

2.3. Synthesis and characterization of biocomposite dispersions

At first, clay was activated with 1N aqueous NaCl. Following stages were performed using this activated clay (NaMt). Cation exchange capacity (CEC) of the clay mineral was determined by methylene blue method. CEC for raw clay mineral was 65 mequiv/100 g clay, however, it was determined as 90 mequiv/100 g clay after activation process. Dispersions which were formed by xylan and NaMt were visually inspected to find critical coagulation concentration (C_k). Different concentrations of xylan (covering 1.0×10^{-9}–5.0×10^{-3} g/ml range) were used with 1.25×10^{-3} g/ml NaMt, but C_k could not be determined. Moreover, solubility of xylan restricted using higher concentrations. Thus maximum xylan concentration without precipitation was 1.00×10^{-2} g/ml. Due to these occasions two routes were followed for synthesis of biocomposites in aqueous media:

(i) NaMt concentration was kept constant at 2.00×10^{-2} g/ml, and xylan concentration was varied covering 7.81×10^{-5}–1.00×10^{-2} g/ml range (Xylan/NaMt dispersions).
(ii) Xylan concentration was kept constant at 1.00×10^{-2} g/ml, and NaMt concentration was varied covering 1.25×10^{-3}–2.00×10^{-2} g/ml range (NaMt/Xylan dispersions).

In both routes components were shaken for 24 h at room temperature. First rheologic measurements of the dispersions performed. Samples of dispersions were dropped on glass plates and let them dried in air for spectral, thermal and morphologic analyses. Then dispersions were centrifuged and electrokinetic measurements were performed from the supernatant.

3. Results and discussion

Critical coagulation concentration for xylan and NaMt dispersions could not be determined. Thus biocomposite dispersions were synthesized changing concentration of one component while the other was kept constant. Synthesized biocomposite dispersions were characterized in terms of their electrokinetic, rheologic, spectral, thermal and morphologic behaviors.

3.1. Electrokinetic and rheologic characterization of biocomposites

Biocomposite dispersions were identified firstly utilizing electrokinetic and rheologic measurements. Electrokinetic measurements were made to see whether xylan was clung onto NaMt surfaces or not. Zeta potential of 2.00×10^{-2} g/ml NaMt dispersion was decreased as absolute value with increasing xylan concentration (Fig. 1a). Zeta potential (which is related with surface charge) of NaMt was −32.40 mV at the beginning; however xylan addition in 7.81×10^{-5}–1.00×10^{-2} g/ml range caused an increase in surface charge up to −11.25 mV, indicating that the dispersion has moved farther from the deflocculated structure. Zeta potential values for NaMt/Xylan dispersions also showed that surface charge has changed indicating surface interaction at first additions. Measurements results of both dispersions were in good agreement, and indicated that a surface interaction took place between xylan and NaMt. These results showed that xylan hang on to NaMt surfaces, but could not cover all.

Viscosities of the biocomposite dispersions showed a tendency to increase uniformly with increasing component concentration. Flow behaviors of NaMt and xylan changed in both routes, due to interactions between each other (Tables 1 and 2). Flow behavior of the both dispersions can be determined from shear stress versus shear rate plot (Fig. 1b). The Xylan/NaMt showed dilatant flow behavior up to 5.00×10^{-3} g/ml xylan addition. After this point

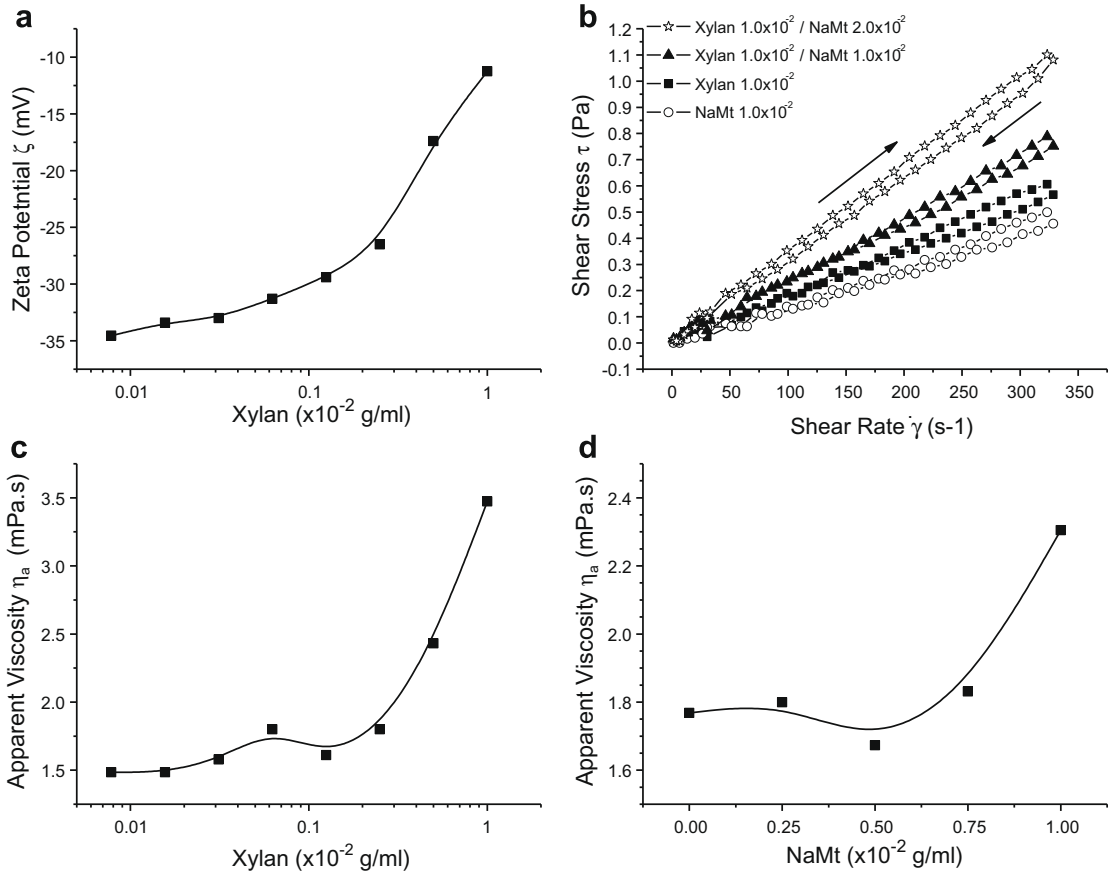

Fig. 1. Change in zeta potential of 2.00×10^{-2} g/ml NaMt with increasing xylan concentration (a), shear stress–shear rate plots (b) apparent viscosity (c and d) of Xylan/NaMt and NaMt/Xylan dispersions.

Table 1
Rheology of Xylan/NaMt dispersions (NaMt was kept at 2.0×10^{-2} g/ml).

Xylan (g/ml)	Apparent viscosity, η_a (mPa s)	Plastic viscosity η_{pl} (mPa s)	Yield value τ_B (mPa)	Hysteresis area (Pa/s)
0.00	1.389	nd[a]	nd[a]	6.985
7.81×10^{-5}	1.484	nd[a]	nd[a]	nd[a]
1.65×10^{-4}	1.484	nd[a]	nd[a]	0.086
3.13×10^{-4}	1.579	nd[a]	nd[a]	1.082
6.25×10^{-4}	1.800	nd[a]	nd[a]	10.238
1.25×10^{-3}	1.610	nd[a]	nd[a]	5.960
2.50×10^{-3}	1.800	nd[a]	nd[a]	8.108
5.00×10^{-3}	2.431	2.377	5.430	16.791
$l.00 \times 10^{-2}$	3.473	3.338	19.450	14.837

[a] Not determined.

Table 2
Rheology of NaMt/Xylan dispersions (xylan was kept at 1.0×10^{-2} g/ml).

NaMt (g/ml)	Apparent viscosity η_a (mPa s)	Plastic viscosity η_{pl} (mPa s)	Yield value τ_B (mPa)	Hysteresis area (Pa/s)
2.00×10^{-2}	3.473	3.338	19.450	14.837
1.50×10^{-2}	3.378	2.974	48.622	7.612
$l.00 \times 10^{-2}$	2.778	2.613	22.725	3.985
7.50×10^{-3}	2.652	2.420	22.753	1.092
5.00×10^{-3}	2.399	2.260	11.326	2.890
2.50×10^{-3}	2.115	2.158	nd[a]	4.667
1.25×10^{-3}	1.894	1.932	0.104	3.504
0.00	1.831	1.767	3.568	4014

[a] Not determined.

flow characteristic was changed to Bingham plastic. Yield value (τ_B), which is an indicator of the interactions between NaMt particles and xylan, could be observed at higher concentrations. Also plastic viscosity (η_{pl}) values have increased as component concentrations went higher, supporting the increase in τ_B. When rheologic parameters compared, both 2.00×10^{-2} g/ml NaMt dispersion, and

1.00×10^{-2} g/ml xylan solution showed dilatant flow model characteristics. However, as xylan and NaMt interacted, the flow model of the composite dispersions changed its characteristic to Bingham plastic.

Apparent viscosity (η_a) is a measure of these interactions (Fig. 1c and d). Rheologic properties of Xylan/NaMt composites were not change up to 1.25×10^{-3} g/ml xylan concentration. However, after this point, interactions increased and a more viscous structure formed. NaMt/Xylan biocomposites also showed similar flow behaviors like Xylan/NaMt dispersions.

Hysteresis area, which is a measure of thixotropy, was calculated from the area under curve of the shear stress–shear rate plot. Both dispersions showed similar thixotropic behaviors with increasing component concentrations. Results obtained from the plots indicated that dispersions' flow behavior changed from dilatant to Bingham plastic and thixotropy increased related with amount of component added.

3.2. Spectral characterization of biocomposites

X-ray diffraction analysis (XRD) was used to determine the interactions between NaMt layers and xylan utilizing basal spacing values (d_{001}) (Pinnavaia & Beall, 2000). Intercalation of NaMt with xylan was very small at the beginning and basal spacing of NaMt (1.260 nm) was increased about 0.03 nm with first additions. But the highest concentration of xylan (1.00×10^{-2} g/ml) intercalated NaMt, extending the basal spacing about 0.36 nm (Fig. 2a). This indicated that xylan was orientated into the interlayer galleries. For NaMt/Xylan dispersions, basal spacing peak could not be determined in first additions of NaMt until the concentration was 5.00×10^{-3} g/ml. The characteristic peak could be identified after NaMt concentration was 7.50×10^{-3} g/ml. Electrokinetic and rheologic data indicated that interactions took place on the surface as NaMt concentration went higher. XRD data also supported this information. At 7.50×10^{-3} g/ml NaMt concentration maximum d_{001} measured as 2.076 nm with an extension of 0.82 nm. Further additions caused to decrease in d_{001} and it was measured about 1.5 nm. This decrease mainly caused from the interactions occurred on the surface rather than interlayer galleries, causing NaMt layers to compact.

Interactions between NaMt and xylan were studied using FTIR spectra (Fig. 2b). Characteristic absorption bands of NaMt determined as structural (3627 cm^{-1}) and intra/intermolecular hydrogen bonded (3453 cm^{-1}) O–H stretching vibrations, H–O–H deformation vibration due to adsorbed water at 1635 cm^{-1}, Si–O stretching vibration at 1033 cm^{-1} with a shoulder at 1087 cm^{-1}, Al–OH (917 and 622 cm^{-1}) and (Al, Mg)–O (848 and 793 cm^{-1}) vibrations modes, Si–O bending vibration at 521 and 467 cm^{-1} (Alemdar, Güngör, Ece, & Atici, 2005; Marel & Beutelspacher, 1976). Typical bands for xylans are O-H stretching as a broad band at 3400 cm^{-1}, aliphatic C–H stretching at 2928 cm^{-1}, H-O-H deformation aroused from adsorbed water at 1627 cm^{-1}, various C–O, C–C stretching and C–O–H, C–O–C bending vibrations in 1200–920 cm^{-1} range (Kacurakova et al., 1999, 2000). C–O–H bending band at 1075 cm^{-1} was strongly influenced by branching (Sun, Tomkinson, Ma, & Liang, 2000). The sharp band at 898 cm^{-1} was an indicator of β-glycosidic bond. Low intensity shoulder at 1154 cm^{-1} was an evidence of arabinosyl side chains.

FTIR spectra of Xylan/NaMt biocomposite samples began to reveal C–H stretching vibrations of xylan at 2924 cm^{-1} as the concentration of added xylan was 6.25×10^{-4} g/ml and above. Moreover, Si–O stretching bands shifted to greater wave numbers indicating interactions became stronger and they were observed at 1038 and 1086 cm^{-1} for the highest xylan concentration (1.00×10^{-2} g/ml). There were no significant changes in structural and inter/intramolecular O-H stretching bands until 6.25×10^{-4} g/ml.

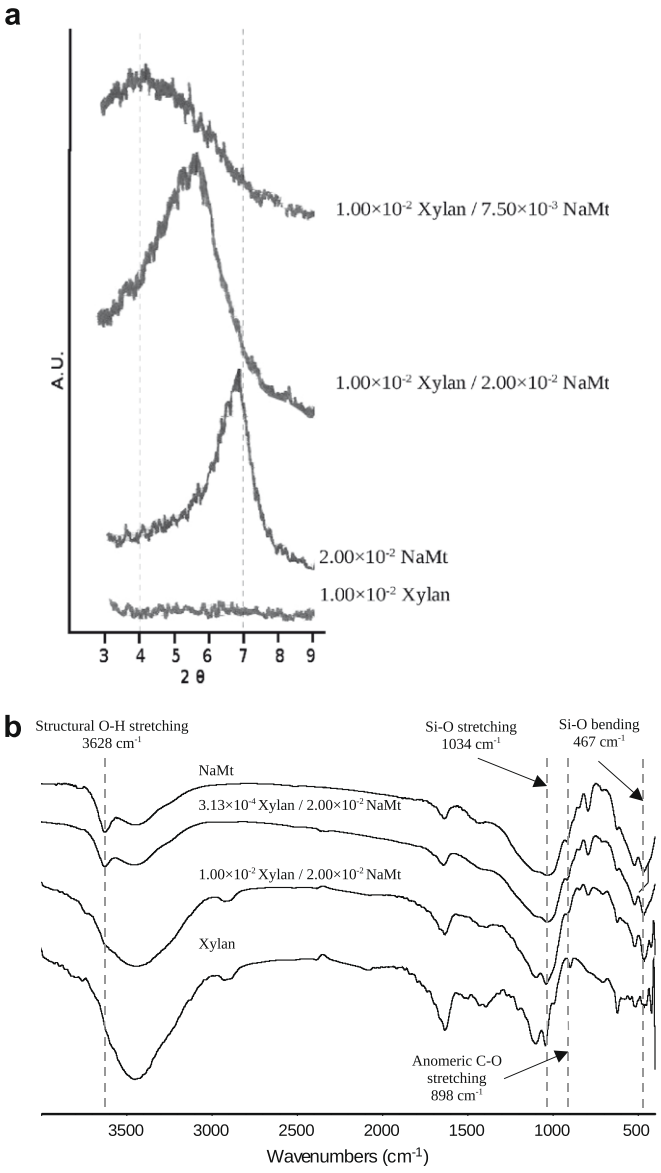

Fig. 2. XRD patterns (a) and FTIR spectrums (b) of biocomposites.

However, after this point there was an increase in the frequency of structural O–H vibration at 3627 cm^{-1} until the concentration was 2.50×10^{-3} g/ml where had the maximum value (3636 cm^{-1}). Then as the concentration increased, both intensity and wave number of this signal decreased. This was an evidence of interaction with structural O–H groups of NaMt with xylan. H–O–H deformation (1635 cm^{-1}) was also shifted to greater frequencies with first additions; however it had nearly constant value after 1.25×10^{-3} g/ml xylan concentration. Si-O stretching vibrations shifted to greater frequencies when the added xylan concentration was smaller than 1.25×10^{-3} g/ml; due to surface adsorption. Further additions of xylan shifted Si–O stretching to smaller wave numbers due to intercalation of NaMt. Also band at 1087 cm^{-1} for 1.00×10^{-2} g/ml xylan concentration was an indication of newly formed Si–O–C bonds between NaMt and xylan. (Al, Mg)-OH vibration modes at 848 and 793 cm^{-1} first shifted to greater wave numbers as a result of surface adsorption, and then they moved to smaller wave numbers. These changes were indications of both surface adsorption and intercalation. Al–OH vibration mode at 917 cm^{-1} shifted to greater wave numbers constantly

after xylan concentration was 1.25×10^{-3} g/ml. FTIR data showed that, when xylan concentration was equal or smaller than 1.25×10^{-3} g/ml mainly surface adsorption occurred on NaMt. However, xylan was intercalating NaMt and forming Si–O–C bonds with O–H groups, which were located in interlayer galleries, for higher xylan concentrations.

FTIR data for NaMt/Xylan samples was also evaluated. As can be seen from the spectra, xylan's local signals around 1000 cm^{-1} changed to Si–O stretching, (Al, Mg)–O vibration modes slowly. Especially structural O–H stretching of NaMt at 3627 cm^{-1} could not be determined as a separate band, only observed as a shoulder to H-bonded O-H groups. Peak maximum of O–H stretching was fluctuated randomly regarding to hydrogen bonds in the samples. Signal at 1634 cm^{-1} (adsorbed water) moved to 1632 cm^{-1} with first additions of NaMt then further additions drifted it to greater frequencies. Region (1500–850 cm^{-1}), which contains various C–O, C–C stretching and C–O–C, C–O–H bending vibrations, increased until NaMt concentration was between 5.00×10^{-3}–1.00×10^{-2} g/ml, then they remained unchanged. Si–O bending decreased to 463 cm^{-1}, whereas remaining peaks tended to drift to greater frequencies.

Results which were obtained from rheologic, spectral and electrokinetic measurements are illustrated in Fig. 3. When NaMt dispersion and xylan solution were mixed a surface interaction between NaMt and xylan occurred. Then this surface interaction could lead either an agglomerate formation or intercalation. Surface-bound xylan chains could interact with each other causing agglomeration of clay particles. However, some xylan chains could intercalate NaMt related with xylan and NaMt concentrations.

3.3. Thermal characterization of biocomposites

Thermal analyses were performed using differential scanning calorimeter (DSC) and thermogravimetric analysis (TGA). Thermograms were shown in Fig. 4a and b and results were summarized in Table 3. Xylan have endothermic and exothermic signals which were regarded as water loss as an endothermic peak at 147.59 °C and thermal degradation as an exothermic peak at 253.49 °C (Beall & Eickner, 1970). NaMt showed an endothermic peak at 185.52 °C which was also attributed to water loss from the surface (Meyers & Speyer, 2003). First Xylan/NaMt systems were evaluated. Xylan-NaMt interaction caused changes these peak positions starting from the first additions. When xylan was 2.50×10^{-3} g/ml, water loss peak divided into two maxima indicating two kinds of interaction. As the concentration increased, endothermic peak of NaMt moved swiftly to lower temperatures. Same peak showed a different behavior in NaMt/Xylan systems. It was rose until 7.50×10^{-3} g/ml, and then dropped down with increasing NaMt. For both systems exothermic signal, which was an indication of thermal decomposition of xylan, moved ca. 300 °C with first additions of NaMt.

When DSC data for NaMt/Xylan dispersions were evaluated, it has been observed that maximum weight loss temperatures in these regions were increased until NaMt concentration was between 7.50×10^{-3} and 1.00×10^{-2} g/ml, then decreased even the concentration increased. These results indicated that thermal stability of xylan has increased with addition of NaMt.

Temperature, which maximum weight loss occurred, has changed with xylan content of Xylan/NaMt dispersion. Weight loss of xylan between 200 and 400 °C could be clearly seen from the thermograms, whereas NaMt did not show any weight loss in this region. However, NaMt has lost only 12% in 20–800 °C region and this weight loss was mainly between 500 and 700 °C.

An increase was observed for maximum weight loss value in both biocomposite dispersions. This increase was not regular in Xylan/NaMt dispersions up to 1.25×10^{-3} g/ml, and then there was a regular rise from 284 to 296 °C in maximum weight loss temperature due to interaction between NaMt and xylan. As zeta potential, rheology and spectral analyses supported that interactions between NaMt and xylan occurred at both interlayer galleries and surfaces after this concentration.

Weight losses at 400 °C and 15% weight loss temperatures were determined for the dispersions. Only 35% residue was observed for xylan, however, as NaMt content increased thermal stability of the xylan also increased. Fifteen percent weight loss temperature increased with increasing NaMt and temperature difference between the highest (1.00×10^{-2} g/ml) and the lowest (7.81×10^{-5} g/ml) concentrations was more than 300 °C. The highest thermal stabilization obtained with the lowest xylan content, where interactions were mainly on the surface. When intercalated species compared (2.50×10^{-3}–1.00×10^{-2} g/ml) it has been observed that thermal stability was much better than xylan.

If DSC and TGA analyses were evaluated together it was obvious that NaMt and xylan formed a new dispersion with different thermal behaviors.

3.4. Morphology of biocomposites

Fig. 5 shows SEM images of biocomposite dispersions. SEM measurements supported the results which were obtained from other analyses. NaMt layers and basal spacing between layers can be clearly seen in Fig. 5a. Addition of NaMt in equal amount (1.00×10^{-2} g/ml) of xylan caused surface interaction and covered NaMt layers. Also results of some interactions were observed between interlayer galleries of NaMt and xylan chains (Fig. 5b). As NaMt concentration was decreased to 7.5×10^{-3} g/ml intercalation of NaMt by xylan chains became dominant, relying on XRD data (Fig. 5c). Xylan interacted mainly with surface of NaMt, and surface and interface of NaMt was covered with xylan. Thus NaMt particles interacted with each other leading flocculation. This flocculation was also observed with SEM, and caused characteristic XRD peak of NaMt became broader. Also these interactions leaded an increase in Bingham yield value and flocculation caused an increase in viscosity, regarding to NaMt and xylan alone.

Surface and interfaces of NaMt was covered with xylan when NaMt concentration was 5.0×10^{-3} g/ml (Fig. 5d). Also characteristic peak of NaMt could not be observed in XRD pattern. This was probably due to surrounding of NaMt with xylan. This event

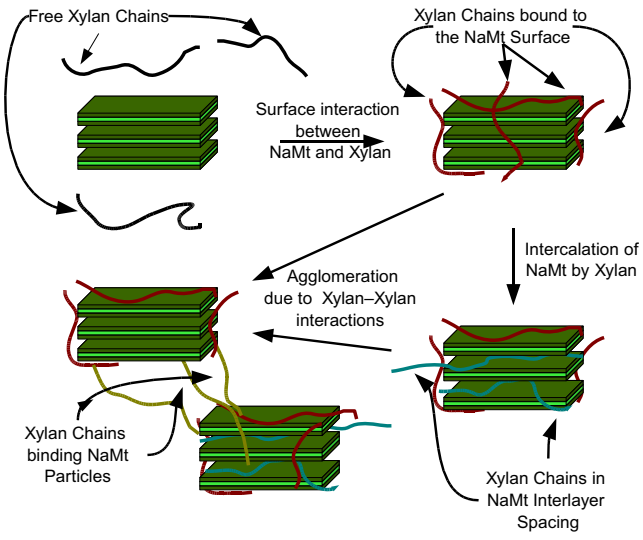

Fig. 3. Schematic representation of intercalation of NaMt by xylan chains.

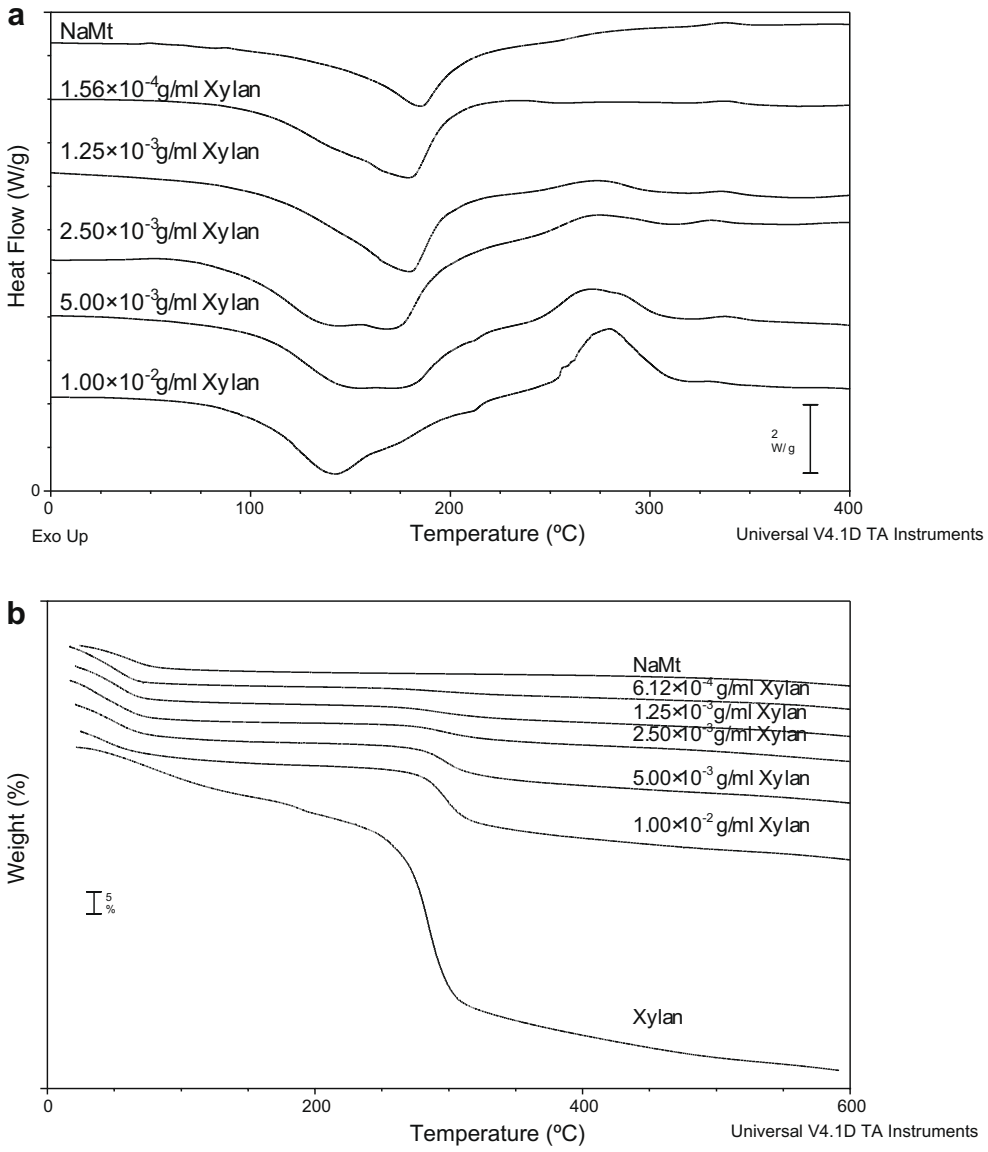

Fig. 4. DSC and TGA thermograms of biocomposite dispersions.

also caused XRD peak became broaden and a decrease of its intensity.

4. Conclusion

Critical coagulation concentration (C_k) of biocomposites dispersions could not be determined. Thus biocomposite synthesis was carried out in two ways. First NaMt concentration was kept constant while xylan's was changing. Then xylan concentration was kept constant while NaMt was changing. At neutral pH xylan's solubility in water was observed as 1 g/100 ml. Solubility problems were observed for xylan at higher concentrations. Due to this limitation experiments were done using 1 g/100 ml as a maximum concentration for xylan. Also flow behavior of NaMt was determined as Bingham plastic up to 2 g/100 ml.

Electrokinetic and rheologic measurements exhibited an interaction started with first additions between NaMt and xylan particles. Zeta potential measurements showed that interactions were on the surface at the beginning. This result also supported with XRD data indicated that xylan chains were not oriented into the interlayer galleries, relying on basal spacing values. Basal spacing values were not changed at the beginning, so this result leaded to a conclusion that interactions were on the NaMt surface mainly. In Xylan/NaMt dispersions, some interactions also started between interlayer galleries of NaMt when xylan concentration exceeded 1.25×10^{-3} g/ml, leading to an increase in basal spacing. The highest xylan concentration, which was used, extended basal spacing by 0.36 nm. On the other hand, in NaMt/Xylan dispersions, which xylan concentration was higher than NaMt concentration, interactions with interlayer galleries were higher. The highest d_{001} measured for these dispersions was 2.08 nm (an increase of 0.82 nm) at 7.50×10^{-3} g/ml NaMt concentration. Basal spacing peak could not be observed at lower NaMt concentrations. The loss of basal spacing peak may be contributed as an indication of that NaMt surfaces were covered with xylan chains.

FTIR data were in good agreement with electrokinetic, rheologic and XRD measurements. For Xylan/NaMt dispersions they indicated that xylan and NaMt particles were interacting on the surface while xylan concentration was lower than 1.25×10^{-3} g/ml. As xylan concentration went higher (especially at 2.50×10^{-3} g/ml or

Table 3
DSC and TGA data for biocomposite systems.

Xylan (g/ml)	NaMt (g/ml)	Endo. peak (°C)	Exo. peak (°C)	T_{max}[a] (°C)	W_{400}[b] (%)	T_{15}[c] (°C)
Xylan/NaMt systems						
0.00	200×10^{-2}	185.5	nd[e]	nd[e]	93.2	nd[e]
7.81×10^{-5}	200×10^{-2}	183.8	226.6	303.2	89.2	712.2
3.13×10^{-4}	200×10^{-2}	174.7	283.0	282.0	88.2	620.4
6.25×10^{-4}	200×10^{-2}	172.2	278.2	292.7	88.5	621.2
1.25×10^{-3}	200×10^{-2}	179.6	273.5	290.9	87.3	561.7
2.50×10^{-3}	200×10^{-2}	144.1, 167.5[d]	274.7	295.5	85.4	426.5
5.00×10^{-3}	200×10^{-2}	156.4, 170.9[d]	271.1	296.3	81.7	311.2
1.00×10^{-2}	200×10^{-2}	143.0	279.7	296.2	75.8	296.6
NaMt/Xylan systems						
1.00×10^{-2}	1.50×10^{-2}	93.8	292.9	290.9	77.5	300.3
1.00×10^{-2}	1.00×10^{-2}	117.7	293.3	296.3	69.4	280.3
1.00×10^{-2}	7.50×10^{-3}	134.6	288.5	302.1	67.5	284.1
1.00×10^{-2}	5.00×10^{-3}	97.5	303.6	302.0	58.7	272.8
1.00×10^{-2}	2.50×10^{-3}	84.4	293.9	300.7	55.0	269.7
1.00×10^{-2}	1.25×10^{-3}	135.6	294.6	302.0	53.1	271.5
1.00×10^{-2}	0.00	147.6	253.5	284.4	35.0	200.7

[a] Temperature which is maximum weight loss observed for xylan.
[b] Residue at 400 °C.
[c] Temperature which is 15% weight loss occured.
[d] Two maxima have been observed.
[e] Not determined.

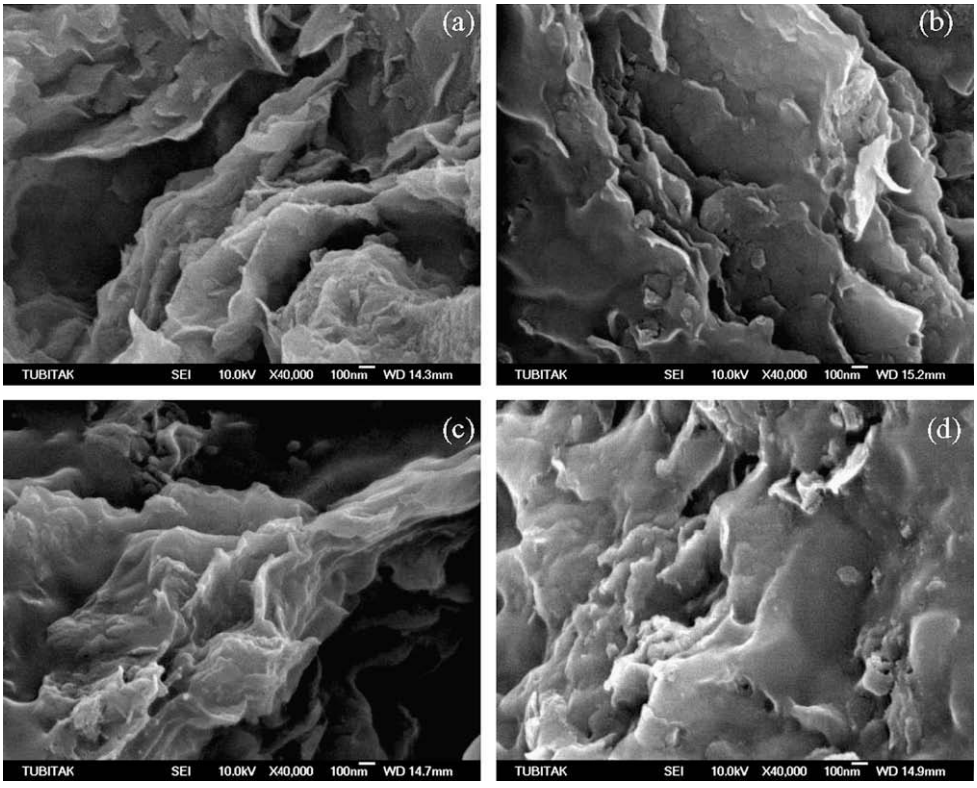

Fig. 5. SEM images of NaMt/Xylan dispersions, (NaMt:Xylan, both $\times 10^{-2}$ g/ml) (a) 2.00:0.00, (b) 1.00:1.00, (c) 0.75:1.00, and (d) 0.50:1.00, respectively.

above), xylan also interacted with interlayer galleries and started intercalation of NaMt. Also NaMt/Xylan dispersions showed surface interaction at the beginning. However, after 7.50×10^{-3} g/ml NaMt concentration, intercalation of NaMt was observed. This could be seen from the signals at 1086 and 842 cm^{-1} regarded as newly formed Si–O–C bonds. In both dispersions xylan obtained a great thermal stability. SEM measurements supported that interactions were mainly at the surface. SEM images indicate some flocculation has occurred due to surface interactions. At lower NaMt concentrations xylan has covered the NaMt surface, causing NaMt particles to form flocculated structures. Thus XRD signals were broadened and their intensity also decreased. Due to these results characteristic NaMt peak could not be observed in XRD pattern. For xylan, both maximum weight loss temperature and residue amount at higher temperatures increased with addition of NaMt. Optimum concentrations for biocomposite dispersions obtained from xylan and NaMt were determined as 1.00×10^{-3} g/ml for each. As a conclusion these biocomposites can found application especially in cosmetics formulations, as both thickener, and cleaner agent.

Acknowledgments

This paper is supported by Research Fund of Istanbul Technical University, Turkey (Project No: 32044). The authors wish to thank to Prof. Dr. Ö. Işık Ece for XRD spectrum measurements.

References

Alemdar, A., Güngör, N., Ece, O. I., & Atici, O. (2005). The rheological properties and characterization of bentonite dispersions in the presence of non-ionic polymer PEG. *Journal of Materials Science, 40*(1), 171–177.

Beall, F. C., & Eickner, H. W. (1970). *Thermal degradation of wood components*. Madison, Wisconsin: US Department of Agriculture, Forest Service, Forest Products Laboratory (p. 29).

Blumenkrantz, N., & Asboe-Hansen, G. (1973). New method for quantitative determination of uronic acids. *Analytical Biochemistry, 54*, 484–489.

Doner, L. W., & Hicks, K. B. (1997). Isolation of hemicellulose from corn fiber by alkaline hydrogen peroxide extraction. *Cereal Chemistry, 74*(2), 176–181.

Ebringerová, A., Hromádková, Z., & Heinze, T. (2005). Hemicellulose. *Advances in Polymer Science, 186*, 1–67.

Eremeeva, T. E., & Bykova, T. O. (1993). High-performance size-exclusion chromatography of wood hemicelluloses on a poly(2-hydroxyethyl methacrylate-co-ethylene dimethacrylate) column with sodium hydroxide solution as eluent. *Journal of Chromatography, 639*, 159–164.

Fahmy, T. Y. A., & Mobarak, F. (2008). Nanocomposites from natural cellulose fibers filled with kaolin in presence of sucrose. *Carbohydrate Polymers, 72*(4), 751–755.

Gáspár, M., Juhász, T., Szengyel, Z., & Réczey, K. (2005). Fractionation and utilisation of corn fibre carbohydrates. *Process Biochemistry, 40*, 1183–1188.

Günister, E., Pestreli, D., Ünlü, C. H., Atıcı, O., & Güngör, N. (2007). Synthesis and characterization of chitosan-MMT biocomposite systems. *Carbohydrate Polymers, 67*(3), 358–365.

Hromadkova, Z., Kovacikova, J., & Ebringerova, A. (1999). Study of the classical and ultrasound-assisted extraction of the corn cob xylan. *Industrial Crops and Products, 9*, 101–109.

Kacuráková, M., Belton, P. S., Wilson, R. H., Hirsch, J., & Ebringerová, A. (1998). Hydration properties of xylan-type structures: An FTIR study of xylooligosaccharides. *Journal of the Science of Food and Agriculture, 77*(1), 38–44.

Kacurakova, M., Capek, P., Sasinkova, V., Wellner, N., & Ebringerova, A. (2000). FT-IR study of plant cell wall model compounds: Pectic polysaccharides and hemicelluloses. *Carbohydrate Polymers, 43*, 195–203.

Kacurakova, M., Wellner, N., Ebringerova, A., Hromadkova, Z., Wilson, R. H., & Belton, P. S. (1999). Characterisation of xylan-type polysaccharides and associated cell wall components by FT-IR and FT-Raman spectroscopies. *Food Hydrocolloids, 13*(1), 35–41.

Marel, H. W. v. d., & Beutelspacher, H. (1976). *Atlas of infrared spectroscopy of clay minerals and their admixtures*. Amsterdam: Elsevier Scientific Pub. Co.

Meyers, K. S., & Speyer, R. F. (2003). Thermal analysis of clays. In M. E. Brown & P. K. Gallagher (Eds.), *Handbook of thermal analysis and calorimetry* (pp. 261–306). New York: Elsevier.

Pinnavaia, T. J., & Beall, G. W. (2000). *Polymer–clay nanocomposites*. Chichester: John Wiley & Sons Ltd.

Ray, S. S., & Bousmina, M. (2005). Biodegradable polymers and their layered silicate nanocomposites: In greening the 21st century materials world. *Progress in Materials Science, 50*(8), 962–1079.

Ray, S. S., & Okamoto, M. (2003). Polymer/layered silicate nanocomposites: A review from preparation to processing. *Progress in Polymer Science, 28*(11), 1539–1641.

Sun, R. C., & Tomkinson, J. (2002). Characterization of hemicelluloses obtained by classical and ultrasonically assisted extractions from wheat straw. *Carbohydrate Polymers, 50*, 263–271.

Sun, R. C., Tomkinson, J., Ma, P. L., & Liang, S. F. (2000). Comparative study of hemicelluloses from rice straw by alkali and hydrogen peroxide treatments. *Carbohydrate Polymers, 42*, 111–122.